ARMY RESEARCH LABORATORY

Optimal Pulse Shapes for SHPB Tests on Soft Materials

by Mike Scheidler, John Fitzpatrick, and Reuben Kraft

ARL-RP-348 **December 2011**

A reprint from the *Proceedings of the 2011 SEM Annual Conference and Exposition on Experimental and Applied Mechanics*, Uncasville, CT, 13–16 June 2011.

NOTICES

Disclaimers

The findings in this report are not to be construed as an official Department of the Army position unless so designated by other authorized documents.

Citation of manufacturer's or trade names does not constitute an official endorsement or approval of the use thereof.

Destroy this report when it is no longer needed. Do not return it to the originator.

Army Research Laboratory
Aberdeen Proving Ground, MD 21005-5069

ARL-RP-348 **December 2011**

Optimal Pulse Shapes for SHPB Tests on Soft Materials

Mike Scheidler, John Fitzpatrick, and Reuben Kraft
Weapons and Materials Research Directorate, ARL

A reprint from the *Proceedings of the 2011 SEM Annual Conference and Exposition on Experimental and Applied Mechanics*, Uncasville, CT, 13–16 June 2011.

REPORT DOCUMENTATION PAGE

Form Approved
OMB No. 0704-0188

1. REPORT DATE *(DD-MM-YYYY)*	2. REPORT TYPE	3. DATES COVERED (From - To)
December 2011	Reprint	October 2010–March 2011

4. TITLE AND SUBTITLE
Optimal Pulse Shapes for SHPB Tests on Soft Materials

5a. CONTRACT NUMBER

5b. GRANT NUMBER

5c. PROGRAM ELEMENT NUMBER

6. AUTHOR(S)
Mike Scheidler, John Fitzpatrick, and Reuben Kraft

5d. PROJECT NUMBER
AH80

5e. TASK NUMBER

5f. WORK UNIT NUMBER

7. PERFORMING ORGANIZATION NAME(S) AND ADDRESS(ES)
U.S. Army Research Laboratory
ATTN: RDRL-WMP-B
Aberdeen Proving Ground, MD 21005-5069

8. PERFORMING ORGANIZATION REPORT NUMBER
ARL-RP-348

9. SPONSORING/MONITORING AGENCY NAME(S) AND ADDRESS(ES)

10. SPONSOR/MONITOR'S ACRONYM(S)

11. SPONSOR/MONITOR'S REPORT NUMBER(S)

12. DISTRIBUTION/AVAILABILITY STATEMENT
Approved for public release; distribution is unlimited.

13. SUPPLEMENTARY NOTES
A reprint from the *Proceedings of the 2011 SEM Annual Conference and Exposition on Experimental and Applied Mechanics*, Uncasville, CT, 13–16 June 2011.

14. ABSTRACT
For split Hopkinson pressure bar (SHPB) tests on soft materials, the goals of homogeneous deformation and uniform uniaxial stress in the specimen present experimental challenges, particularly at higher strain rates. It has been known for some time that attainment of these conditions is facilitated by reducing the thickness of the specimen or by appropriately shaping the loading pulse. Typically, both methods must be employed. Pulse shapes are often tailored to deliver a smooth and sufficiently slow rise to a constant axial strain rate, as this promotes equality of the mean axial stress on the two faces of the specimen, a condition referred to as dynamic equilibrium. However, a constant axial strain rate does not eliminate radial acceleration, which may result in large radial and hoop stresses and large radial variations in the radial, hoop and axial stresses. An approximate analysis (assuming homogeneous deformation and incompressibility) indicates that these radial inertia effects would be eliminated if the radial strain rate were constant. Motivated by this result, we consider loading pulses that deliver a constant radial strain rate after an initial ramp-up. The corresponding axial strain rate is no longer constant on any time interval, but for sufficiently thin specimens the resulting departure from dynamic equilibrium may be small enough to be tolerable. This is explored here by comparing the analytical predictions for the conventional and "optimal" loading pulse shapes with corresponding numerical simulations of SHPB tests on a soft, nearly incompressible material.

15. SUBJECT TERMS
high strain rate, soft materials, Hopkinson bar, inertial effects, pulse shaping

16. SECURITY CLASSIFICATION OF:			17. LIMITATION OF ABSTRACT	18. NUMBER OF PAGES	19a. NAME OF RESPONSIBLE PERSON
a. REPORT	b. ABSTRACT	c. THIS PAGE			Mike Scheidler
Unclassified	Unclassified	Unclassified	UU	20	19b. TELEPHONE NUMBER (*Include area code*) 410-278-5436

Optimal Pulse Shapes for SHPB Tests on Soft Materials

Mike Scheidler, John Fitzpatrick and Reuben Kraft
Weapons and Materials Research Directorate
U.S. Army Research Laboratory
Aberdeen Proving Ground, MD 21005-5066

ABSTRACT For split Hopkinson pressure bar (SHPB) tests on soft materials, the goals of homogeneous deformation and uniform uniaxial stress in the specimen present experimental challenges, particularly at higher strain rates. It has been known for some time that attainment of these conditions is facilitated by reducing the thickness of the specimen or by appropriately shaping the loading pulse. Typically, both methods must be employed. Pulse shapes are often tailored to deliver a smooth and sufficiently slow rise to a constant axial strain rate, as this promotes equality of the mean axial stress on the two faces of the specimen, a condition referred to as dynamic equilibrium. However, a constant axial strain rate does not eliminate radial acceleration, which may result in large radial and hoop stresses and large radial variations in the radial, hoop and axial stresses. An approximate analysis (assuming homogeneous deformation and incompressibility) indicates that these radial inertia effects would be eliminated if the *radial* strain rate were constant. Motivated by this result, we consider loading pulses that deliver a constant radial strain rate after an initial ramp-up. The corresponding axial strain rate is no longer constant on any time interval, but for sufficiently thin specimens the resulting departure from dynamic equilibrium may be small enough to be tolerable. This is explored here by comparing the analytical predictions for the conventional and "optimal" loading pulse shapes with corresponding numerical simulations of SHPB tests on a soft, nearly incompressible material.

1. Introduction

The split Hopkinson pressure bar (SHPB), also known as the Kolsky bar, is widely used to characterize the strain rate sensitivity of inelastic materials in a state of compressive uniaxial stress for moderate to large strains. The review articles by Gray [1], Gama et al. [2], and Ramesh [3] and the recent book by Chen and Song [4] are recommended for background on this technique. The standard specimen shape for SHPB tests is solid disk, which (particularly for soft specimens) is relatively thin compared to the diameter in order to reduce axial inertia effects. The analysis and simulations in this paper are confined to this specimen geometry. The standard analysis of SHPB test data relies on the assumption of uniform uniaxial stress and uniform biaxial strain throughout the specimen. These conditions, as well as a nearly constant nominal strain rate, can often be achieved after an initial ring-up. However, a number of technical challenges arise when the specimen is extremely soft; cf. [1]–[4] and also Gray and Blumenthal [5], Chen et al. [6], Song and Chen [7], Moy et al. [8], Song et al. [9], and Sanborn [10].

Inertial effects in soft specimens may result in highly non-uniform conditions and a stress state that is far from uniaxial, particularly if the strain rate is sufficiently high. To minimize the effects of axial inertia, loading pulse shapes are typically tailored to deliver a smooth and sufficiently slow rise to a constant nominal (or engineering) axial strain rate. This promotes axial uniformity of the stress and strain components and, in particular, equality of the mean axial stress on the two faces of the specimen, a condition referred to as dynamic equilibrium. The constant axial strain rate condition also simplifies calibration of constitutive models for which the stress depends explicitly on the strain rate, e.g., plasticity models with rate dependent yield stress. However, a constant nominal axial strain rate does not eliminate the radial acceleration of the specimen, which may result in large radial and hoop stresses and large radial variations in the radial, hoop and axial stresses. Since only the mean axial stress is measured in an SHPB test, the full stress state cannot be inferred in such cases; in particular, the deviatoric stress (which typically exhibits the largest rate effects) cannot be determined. Consequently, the measured axial stress is not useful for constitutive model calibration unless the data can be "corrected" for radial inertia effects.

An approximate analysis (assuming an incompressible specimen that deforms homogeneously) indicates that the radial inertia effects would be eliminated if the nominal *radial* strain rate were constant. Motivated by this result, we

consider loading pulses that deliver a constant nominal radial strain rate after an initial ramp-up. The corresponding axial strain rate is no longer constant on any time interval; in fact, it is necessarily decreasing on the time interval over which the radial strain rate is constant. But for sufficiently thin specimens the resulting departure from dynamic equilibrium may be small enough to be tolerable. This is explored here by comparing the analytical predictions for the conventional and "optimal" loading pulse shapes with corresponding numerical simulations of SHPB tests. An inertial correction for the deviatoric stress is also compared with the deviatoric stress in the simulation.

The analysis on which these the inertial corrections and the optimal loading pulse shapes are based applies only to nearly incompressible specimens, that is, materials for which the bulk modulus is several orders of magnitude larger than the shear modulus. This is not necessarily a drawback, since radial inertia effects are expected to be more pronounced for nearly incompressible specimens. Examples of soft, nearly incompressible materials include many rubbers, biological materials with high fluid content (in particular, brain tissue), and tissue surrogates such as gelatins. The analysis assumes that the specimen is isotropic, although no particular form for the constitutive relation is required. On the other hand, an isotropic, nonlinear elastic constitutive relation was used for the specimen in the numerical simulations, namely, a compressible version of the Mooney-Rivlin model with the bulk modulus of water and a shear modulus typical of a gelatin, so that the ratio of bulk to shear modulus exceeds 10^4.

2. Homogeneous, Axisymmetric Deformations

Our analysis is confined to the deformation and stress in the specimen, which is assumed to be a (relatively thin) solid disc. We use a cylindrical coordinate system aligned with the axis of symmetry of the specimen and the pressure bars. Coordinates of the specimen in the undeformed reference configuration are denoted by (R, Θ, Z); coordinates of the corresponding material point in the deformed state are denoted by (r, θ, z). For a general axisymmetric deformation,

$$r = \hat{r}(R, Z, t)\,, \quad \theta = \Theta\,, \quad z = \hat{z}(R, Z, t)\,, \tag{1}$$

where t denotes time. The radial, hoop, axial and shear components of the Cauchy or true stress tensor $\boldsymbol{\sigma}$ (taken positive in compression) are denoted by σ_{rr}, $\sigma_{\theta\theta}$, σ_{zz} and σ_{rz}. The other two stress components, $\sigma_{r\theta}$ and $\sigma_{z\theta}$, are zero for axisymmetric deformations since the specimen is assumed to be isotropic, but in general (e.g., if the specimen bulges) σ_{rz} need not be zero. The Cauchy stress measures force per unit deformed area. The nominal (engineering, 1st Piola-Kirchhoff) stress tensor $\boldsymbol{\Sigma}$ measures force per unit original (undeformed) area. The axial and radial components of this tensor (which are the only ones referred to in the sequel) are denoted by Σ_{zZ} and Σ_{rR} and are likewise taken positive in compression.

We make the approximation that the specimen deformation is also homogeneous, in which case (1) reduces to

$$r = \lambda_r(t)\,R\,, \quad \theta = \Theta\,, \quad z = \lambda_z(t)\,Z + z_0(t)\,. \tag{2}$$

The initial radius of the specimen is denoted by R_0, and the deformed radius at time t is denoted by $r_0(t)$:

$$r_0(t) = \lambda_r(t)\,R_0 \qquad \text{and} \qquad r/r_0(t) = R/R_0\,. \tag{3}$$

For a material point located initially at radius R, the deformed radius r at time t is given by $(2)_1$, so the radial velocity and acceleration of the specimen at this radial location are given by

$$\dot{r} = \dot{\lambda}_r(t)\,R = \frac{\dot{\lambda}_r(t)}{\lambda_r(t)}\,r\,, \qquad \ddot{r} = \ddot{\lambda}_r(t)\,R = \frac{\ddot{\lambda}_r(t)}{\lambda_r(t)}\,r\,, \tag{4}$$

where a superposed dot denotes a time derivative. At any instant t, the radial velocity and acceleration of the specimen increase linearly with the radius. They are zero on the axis and attain their largest absolute value at the (stress-free) lateral surface, where $\dot{r}_0(t) = \dot{\lambda}_r(t)\,R_0$ and $\ddot{r}_0(t) = \ddot{\lambda}_r(t)\,R_0$. From the relations (2), we have

$$\lambda_r = \frac{\partial r}{\partial R} = \frac{r}{R} =: \lambda_\theta \qquad \text{and} \qquad \lambda_z = \frac{\partial z}{\partial Z}\,. \tag{5}$$

It follows that λ_r, λ_θ and λ_z are the stretches (local ratios of deformed to undeformed length) in the coordinate directions. Since we are concerned with possibly large specimen deformations, we must be careful to distinguish between various finite deformation measures of strain. The two most commonly used measures in the Hopkinson

bar literature are the nominal (or engineering) strain, which is the change in length per unit original length, and the logarithmic (or true) strain. The nominal and logarithmic measures of radial, hoop and axial strain are defined by

$$e_r = 1 - \lambda_r\,, \quad e_\theta = 1 - \lambda_\theta\,, \quad e_z = 1 - \lambda_z\,, \tag{6}$$

and

$$\varepsilon_r = -\ln \lambda_r\,, \quad \varepsilon_\theta = -\ln \lambda_\theta\,, \quad \varepsilon_z = -\ln \lambda_z\,, \tag{7}$$

respectively. Since the radial and hoop stretches are equal, so are the corresponding strains:

$$e_\theta = e_r \quad \text{and} \quad \varepsilon_\theta = \varepsilon_r\,; \tag{8}$$

so we will focus on the radial and axial stretches and strains. The nominal and logarithmic strain measures approach each other in the small strain limit, but differ substantially for large strains. We will work primarily with the nominal strains in this paper, as this simplifies most of the results. Note that stretches are 1 in the undeformed state, greater than 1 in extension, and between 0 and 1 in compression. The strains have been defined so that they are positive if the particular coordinate direction is in compression and negative if it is in extension.[1] In an SHPB test the specimen is compressed in the axial direction, so that $0 < \lambda_z < 1$ and $0 < e_z < 1$. Since the lateral surface is unconfined, the specimen is free to expand radially and we expect that $\lambda_r > 1$ and hence $e_r < 0$. From (6) and (7), we see that the axial strain rates and stretch rates are related by

$$\dot{e}_z = -\dot{\lambda}_z\,, \qquad \dot{\varepsilon}_z = -\frac{\dot{\lambda}_z}{\lambda_z} = \frac{\dot{e}_z}{1 - e_z}\,. \tag{9}$$

Analogous relations hold for the radial strain and stretch rates.

Now consider the stress state. Let p denote the pressure and $\boldsymbol{s}$ the deviatoric part of the Cauchy stress tensor. Then

$$\sigma_{rr} = s_{rr} + p\,, \qquad \sigma_{\theta\theta} = s_{\theta\theta} + p\,, \qquad \sigma_{zz} = s_{zz} + p\,, \tag{10}$$

$$s_{rr} + s_{\theta\theta} + s_{zz} = 0\,, \qquad p = \tfrac{1}{3}\,(\sigma_{zz} + \sigma_{rr} + \sigma_{\theta\theta})\,. \tag{11}$$

Since the radial and hoop stretches coincide and the specimen is isotropic, the radial and hoop stresses are equal and the shear stress is zero:

$$\sigma_{rr} = \sigma_{\theta\theta}\,, \quad \sigma_{rz} = 0\,. \tag{12}$$

Thus a homogeneous axisymmetric deformation results in a biaxial stress and strain state; the principal axes of stress and strain are the axis of symmetry and any axes orthogonal to it. In this case, the relations (11) simplify to

$$s_{rr} = s_{\theta\theta} = -\tfrac{1}{2}\,s_{zz}\,, \qquad p = \tfrac{1}{3}\,(\sigma_{zz} + 2\sigma_{rr})\,. \tag{13}$$

On substituting the relation $(13)_2$ for p into the relation $(10)_3$ for σ_{zz}, we obtain the equivalent relations

$$\sigma_{zz} = \tfrac{3}{2}\,s_{zz} + \sigma_{rr}\,, \qquad s_{zz} = \tfrac{2}{3}\,(\sigma_{zz} - \sigma_{rr})\,. \tag{14}$$

For axisymmetric deformations of an isotropic specimen, the balance of radial momentum is given by[2]

$$\frac{\partial \sigma_{rr}}{\partial r} + \frac{\sigma_{rr} - \sigma_{\theta\theta}}{r} + \frac{\partial \sigma_{rz}}{\partial z} = -\rho\,\ddot{r}\,, \tag{15}$$

where ρ is the density in the deformed state. In view of (12), for homogeneous deformations this reduces to

$$\frac{\partial \sigma_{rr}}{\partial r} = -\rho\,\ddot{r}\,. \tag{16}$$

Since the lateral surface of the specimen is stress free, $\sigma_{rr} = 0$ when $r = r_0(t)$. Then on integrating (16) from an arbitrary radius r to $r_0(t)$ and using (4) and (3), we obtain

$$\sigma_{rr} = 2\,\overline{\sigma}_{rr}(t)\left[1 - \left(\frac{r}{r_0(t)}\right)^2\right] = 2\,\overline{\sigma}_{rr}(t)\left[1 - \left(\frac{R}{R_0}\right)^2\right]\,, \tag{17}$$

[1] The standard sign convention in the continuum mechanics literature takes stress and strain components as positive in tension. The opposite sign convention is typically used in the compression Hopkinson bar literature, and we have followed that convention here.

[2] The minus sign on the right side of (15) is a consequence of the convention that stresses are positive in compression.

where

$$\overline{\sigma}_{rr}(t) = \frac{\rho R_0^2}{4}\,\lambda_r(t)\,\ddot{\lambda}_r(t)\,. \tag{18}$$

Working directly with (17), we find that $\overline{\sigma}_{rr}(t)$ is the mean value of σ_{rr} over the deformed volume of the specimen at time t. Since the deformation is homogeneous, this is also the mean value of σ_{rr} over the undeformed reference configuration. And since σ_{rr} is axially uniform, $\overline{\sigma}_{rr}$ is also the mean value of σ_{rr} over any deformed (z = constant) or undeformed (Z = constant) cross-sectional area. Since $\sigma_{\theta\theta} = \sigma_{rr}$, we conclude that the radial and hoop stresses vary quadratically with the radius but are axially uniform. They attain a peak absolute value of $2\overline{\sigma}_{rr}(t)$ at the centerline ($r = R = 0$) and reduce to zero at the lateral surface. They have the same sign as the radial stretch acceleration $\ddot{\lambda}_r$, but without additional assumptions neither the sign nor the magnitude of $\ddot{\lambda}_r$ can be inferred. In any case, it is clear that the presence of nonzero radial and hoop stresses is a radial inertial effect, that is, a consequence of the fact that the $\rho\ddot{r}$ term in (16) is not necessarily negligible. It follows that in the quasi-static limit, that is, in the limit as $\ddot{r}$ (or $\ddot{\lambda}_r$) approaches zero, $\overline{\sigma}_{rr}(t) = 0$. Hence, as expected, in a quasi-static test we have a uniaxial stress state ($\sigma_{rr} = \sigma_{\theta\theta} = 0$), and by $(13)_2$ and $(14)_2$ the pressure and deviatoric stress are completely determined by the axial stress: $p = \frac{1}{3}\sigma_{zz}$ and $s_{zz} = \frac{2}{3}\sigma_{zz}$. On the other hand, it is clear from $(13)_2$ and $(14)_2$ that these quasi-static estimates for p and s_{zz} will be in error if σ_{rr} is sufficiently large relative to σ_{zz}.

3. The Incompressibility Approximation

The Jacobian of the deformation, denoted by J, is the determinant of the deformation gradient $\boldsymbol{F}$ and represents the local ratio of deformed to undeformed volume. For a general deformation, J is the product of the principal stretches; for a homogeneous axisymmetric deformation this yields $J = \lambda_r\lambda_\theta\lambda_z = \lambda_r^2\lambda_z$. Since the focus of this paper is on nearly incompressible specimens, we will make the approximation that the deformation is volume-preserving. Then $J = 1$, which is equivalent to any of the following relations:

$$\lambda_r = \frac{1}{\sqrt{\lambda_z}}\,, \qquad \lambda_z = \frac{1}{\lambda_r^2}\,, \qquad \varepsilon_r = -\tfrac{1}{2}\,\varepsilon_z\,. \tag{19}$$

Thus the radial stretches or strains are determined by axial stretches or strains, and vice versa. In this case the true and nominal stress components are related by[3]

$$\sigma_{zz} = \lambda_z\Sigma_{zZ} = (1 - e_z)\Sigma_{zZ}\,, \qquad \sigma_{rr} = \lambda_r\Sigma_{rR}\,. \tag{20}$$

Now recall the relations (9) between the axial components of strain rate and stretch rate (with analogous relations for the radial components). By (19) we obtain the following additional relations between the radial and axial rates:

$$-\dot{e}_r = \dot{\lambda}_r = \frac{-\dot{\lambda}_z}{2\lambda_z^{3/2}} = \frac{\dot{e}_z}{2\lambda_z^{3/2}} = \frac{\dot{e}_z}{2(1-e_z)^{3/2}}\,, \qquad \dot{e}_z = -\dot{\lambda}_z = \frac{2\dot{\lambda}_r}{\lambda_r^3}\,, \qquad \dot{\varepsilon}_r = -\tfrac{1}{2}\,\dot{\varepsilon}_z\,. \tag{21}$$

From the relations on the left in (21), we find that the radial strain and stretch accelerations are given in terms of the axial stretch or strain rates by

$$-\ddot{e}_r = \ddot{\lambda}_r = -\frac{1}{2}\frac{\ddot{\lambda}_z}{\lambda_z^{3/2}} + \frac{3}{4}\frac{\left(\dot{\lambda}_z\right)^2}{\lambda_z^{5/2}} = \frac{1}{2}\frac{\ddot{e}_z}{(1-e_z)^{3/2}} + \frac{3}{4}\frac{\left(\dot{e}_z\right)^2}{(1-e_z)^{5/2}}\,. \tag{22}$$

We also have

$$\ddot{\lambda}_r = \frac{1}{\sqrt{\lambda_z}}\left[\frac{1}{2}\,\ddot{\varepsilon}_z + \frac{1}{4}\left(\dot{\varepsilon}_z\right)^2\right]\,, \tag{23}$$

although this relation is less useful than (22). For later use in the discussion of optimal pulse shapes, we note that the nominal axial strain acceleration is given in terms of the radial stretch rates by

$$\ddot{e}_z = -\ddot{\lambda}_z = 2\frac{\ddot{\lambda}_r}{\lambda_r^3} - 6\frac{\left(\dot{\lambda}_r\right)^2}{\lambda_r^4}\,. \tag{24}$$

Now consider the radial stress. Since the deformation is volume-preserving, $\rho = \rho_0$, the density in the undeformed state. On substituting this and the relations $(19)_1$ and (22) for λ_r and $\ddot{\lambda}_r$ into (18), we obtain the following

[3]These relations follow from the general relation $\boldsymbol{\sigma} = J^{-1}\boldsymbol{\Sigma}\boldsymbol{F}^T$, or from the relations between deformed and undeformed area.

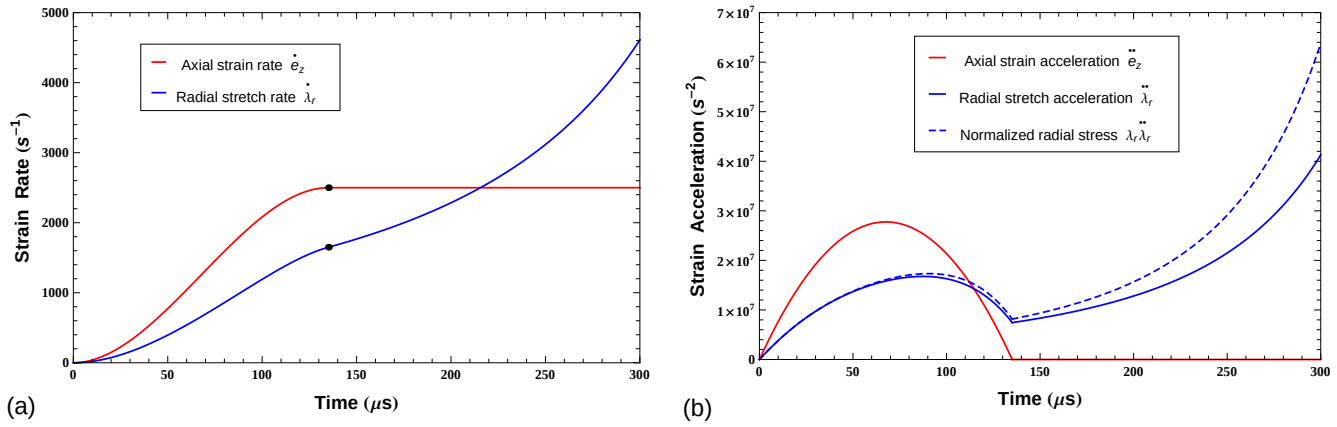

Figure 1: Axial strain and radial stretch rates (a) and accelerations (b) for a smooth ramp-up to a constant nominal *axial* strain rate $\dot{e}_z$ of 2500/s after 135 μs. Also shown in (b) is the normalized mean radial stress (dashed line).

expressions for the mean radial (and hoop) stress in an isotropic specimen undergoing a homogeneous, volume-preserving, axisymmetric deformation:

$$\overline{\sigma}_{rr}(t) \;=\; \frac{\rho_0 R_0^2}{4}\,\lambda_r(t)\,\ddot{\lambda}_r(t) \;=\; \frac{\rho_0 R_0^2}{16}\left[\frac{-2\,\ddot{\lambda}_z}{\lambda_z^2}+\frac{3\big(\dot{\lambda}_z\big)^2}{\lambda_z^3}\right] \;=\; \frac{\rho_0 R_0^2}{16}\left[\frac{2\,\ddot{e}_z}{(1-e_z)^2}+\frac{3\,(\dot{e}_z)^2}{(1-e_z)^3}\right]. \tag{25}$$

The radial (and hoop) stress distribution is then given by (17). For a given radial or axial strain history, we see that the mean radial stress at any instant is proportional to $\rho_0 R_0^2$. Thus radial inertial effects can be reduced by decreasing the radius of the specimen.[4] Note that the only material property appearing in (25) is the density ρ_0; in particular, this estimate for the radial stress is independent of the constitutive relation for the specimen. The relation (17), with $\overline{\sigma}_{rr}(t)$ given by the expression on the right in (25), is equivalent to relations in Dharan and Hauser [11], Warren and Forrestal [12], and Scheidler and Kraft [13].

Now consider a conventional smooth loading pulse for an SHPB test with rise time t_1. We take time $t = 0$ to be the instant at which the loading pulse arrives at the specimen-incident bar interface, so that $e_z(0) = 0$. For a smooth loading pulse the nominal axial strain rate and strain acceleration are initially zero also, $\dot{e}_z(0) = 0$ and $\ddot{e}_z(0) = 0$; and $\dot{e}_z(t)$ increases smoothly with t up to time t_1, after which $\dot{e}_z$ is remains constant at the test strain rate $\dot{e}_{z1} = \dot{e}_z(t_1) > 0$.[5] At early times, the strain acceleration term in (25), $\ddot{e}_z$, dominates as $\dot{e}_z$ increases from its initial value of zero; $\ddot{e}_z$ eventually reaches a peak (positive) value and then decays to zero as $\dot{e}_z$ approaches the plateau strain rate $\dot{e}_{z1}$. This peak in $\ddot{e}_z$ results in a corresponding early peak in the radial stress. However, while the radial stress initially decreases after this peak, it does not decay to zero with $\ddot{e}_z$ since the $(\dot{e}_z)^2$ term in (25) is positive. In fact, since e_z is increasing, the $(1-e_z)^3$ term in the denominator is decreasing, and hence the $3(\dot{e}_z)^2/(1-e_z)^3$ term is strictly increasing, even in the plateau region when $\dot{e}_z(t) = \dot{e}_{z1}$. Consequently, $\overline{\sigma}_{rr}(t)$ begins to increase just prior to time t_1 and continues to do so while $\dot{e}_z$ remains constant, i.e., there is a strain amplification effect on the inertially generated radial stress. These features are illustrated in Figure 1, where the rise time $t_1 = 135$ μs and the plateau value of the nominal axial strain rate is $\dot{e}_{z1} = 2500/\text{s}$. For this strain rate history, $e_z(t_1) = 0.17$ and $e_z(300\mu\text{s}) = 0.58$. Note that by $(25)_1$, the product $\dot{\lambda}_r\ddot{\lambda}_r$ is the mean radial stress $\overline{\sigma}_{rr}$ normalized by the factor $\rho_0 R_0^2/4$; it is this normalized mean radial stress that is plotted in the figure. Also note that by $(25)_1$ and $(20)_2$, the radial stretch acceleration $\ddot{\lambda}_r$ is the mean value of the nominal radial stress Σ_{rR} normalized by the same factor.

For sufficiently soft materials and sufficiently high strain rates, the inertial effects discussed above must be taken into account when analyzing the data from SHPB tests. In this regard, the following relations for the mean values of the stress components are useful:

$$\overline{\sigma}_{zz} = \tfrac{3}{2}\,\overline{s}_{zz} + \overline{\sigma}_{rr}\,, \qquad \overline{s}_{zz} = \tfrac{2}{3}\,(\overline{\sigma}_{zz} - \overline{\sigma}_{rr})\,, \qquad \overline{\sigma}_{zz} = (1-e_z)\,\overline{\Sigma}_{zZ}\,. \tag{26}$$

[4] However, reducing the specimen radius also reduces the signal to the transmission bar, so substantial reduction in specimen size must be accompanied by a corresponding reduction in the diameter of the pressure bars. This is one of the motivations for the use of miniaturized Hopkinson bars.

[5] For simplicity, we neglect the subsequent unloading stage in both the analysis and the numerical simulations.

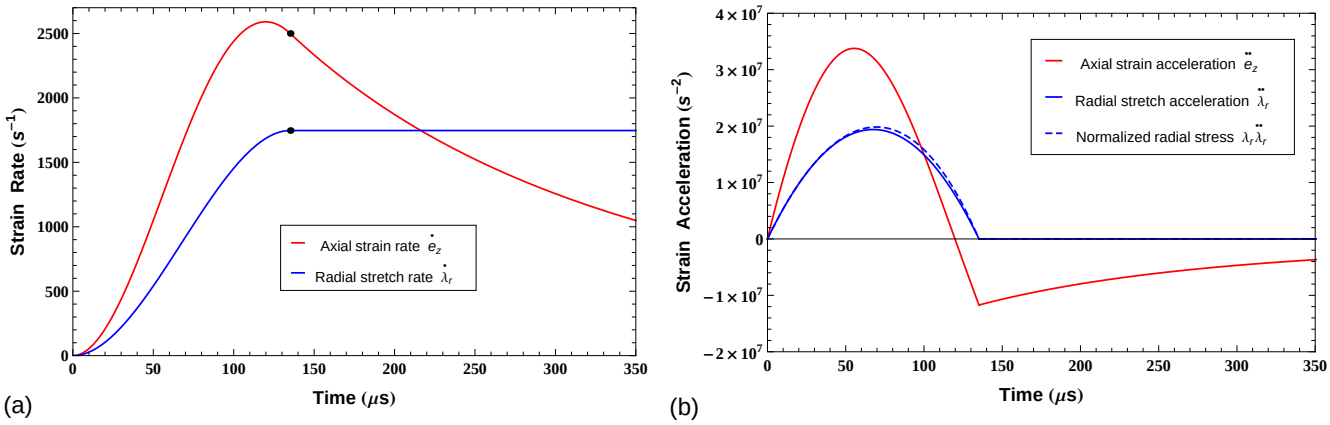

Figure 2: Axial strain and radial stretch rates (a) and accelerations (b) for a smooth ramp-up to a constant nominal *radial* stretch rate of 1747/s after 135 μs. Also shown in (b) is the normalized mean radial stress (dashed line).

These follow from (14) and $(20)_1$, and may be regarded either as volumetric averages or as cross-sectional averages; the two are equivalent if, as will be assumed here, the specimen is in dynamic equilibrium so that the axial stresses are axially uniform. The well-known relation on the right expresses the mean axial Cauchy stress in terms of the axial strain and the mean axial nominal stress, both of which are measured (or inferred from measurements) in an SHPB test. The relation on the left in (26) implies that if the early spike in $\overline{\sigma}_{rr}$ is sufficiently large relative to $\overline{s}_{zz}$ (a situation that could occur for sufficiently high strain rates and sufficiently soft specimens), then a corresponding spike in the measured axial stress is to be expected. These inertial spikes have indeed been observed in SHPB tests on soft, nearly incompressible materials; cf. [4], [8], [9], and [10]. The middle relation in (26), which is equivalent to the relation on the left, indicates that an "inertial correction" must be applied to the (quasi-static) uniaxial stress relation $s_{zz} = \frac{2}{3}\sigma_{zz}$ when $\overline{\sigma}_{rr}$ is sufficiently large. Since $\overline{\sigma}_{rr}$ can be determined from the measured axial strain rate $\dot{e}_z$ by $(25)_3$, the relation $(26)_2$ could provide a means to estimate the axial component of the deviatoric stress,[6] provided the assumptions on which our analysis is based are approximately valid and the difference between $\overline{\sigma}_{zz}$ and $\overline{\sigma}_{rr}$ is not so small that it is in the noise level. Then the radial and hoop components of deviatoric stress can be determined from $(13)_1$.

4. Optimal Loading Pulses

Since a constant nominal axial strain rate does not eliminate inertially generated radial and hoop stresses, it is reasonable to seek axial strain rate histories that do so. On setting $\overline{\sigma}_{rr}(t) = 0$ in (25), we see that the expression on the right yields an ODE for e_z: $2\ddot{e}_z + 3(\dot{e}_z)^2/(1-e_z) = 0$. However, it is simpler to proceed as follows. From $(25)_1$ we see that $\overline{\sigma}_{rr} = 0$ iff $\ddot{\lambda}_r = 0$ iff $\dot{\lambda}_r$ is constant iff $\dot{e}_r$ is constant. Since the loading pulse arrives at $t = 0$ and since $\lambda_r = 1$ in the undeformed state, we take $\lambda_r(0) = 1$. For a smooth loading pulse we cannot impose the constant radial strain rate condition initially. Instead we want $\dot{\lambda}_r(0) = 0$ and $\ddot{\lambda}_r(0) = 0$, with $\dot{\lambda}_r(t)$ increasing smoothly and monotonically with t up to some time t_1, after which $\dot{\lambda}_r$ remains constant:

$$\dot{\lambda}_r(t) = \dot{\lambda}_r(t_1) > 0\,, \quad \text{for } t \geq t_1\,. \tag{27}$$

Then $\lambda_z(t) = 1/\lambda_r^2$ [cf. $(19)_2$], and from λ_z we can determine e_z, $\dot{e}_z$ and $\ddot{e}_z$; alternatively, we can determine $\dot{e}_z$ and $\ddot{e}_z$ directly from λ_r and its rates by using (24) and the middle relation on (21). Since $\dot{\lambda}_r(t)$ is positive for $t > 0$, so is $\dot{e}_z(t)$ [cf. (21)]. However, $\ddot{\lambda}_r(t) = 0$ for $t \geq t_1$, so by (24) we see that $\ddot{e}_z(t) < 0$ for $t \geq t_1$; hence $\dot{e}_z(t)$ is decreasing for $t \geq t_1$. Since the initial condition $\dot{\lambda}_r(0) = 0$ implies $\dot{e}_z(0) = 0$, it follows that $\dot{e}_z(t)$ must increase from zero to a peak value at some time $t_p < t_1$, after which $\dot{e}_z$ decreases. In spite of this non-standard feature, the resulting nominal axial strain rate history $\dot{e}_z(t)$ will have the property that for $t \geq t_1$, $\overline{\sigma}_{rr}(t) = 0$ and hence [cf. (17)] $\sigma_{rr}(r,z,t) = 0$ throughout the specimen.

[6] This is essentially what was done in Sanborn [10] for SHPB tests on various rubbers. His "corrected" axial stress is $\overline{\sigma}_{zz} - \overline{\sigma}_{rr}$ and hence is equivalent to the $\frac{3}{2}\overline{s}_{zz}$ term in $(26)_1$.

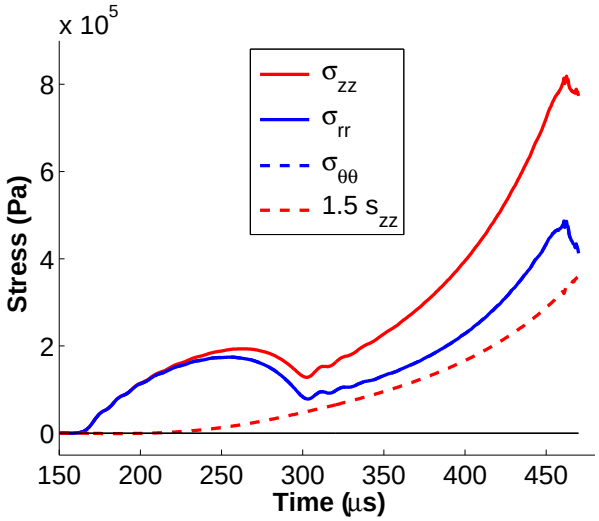

Figure 3: Mean values of the axial, radial and hoop stress and of 3/2 the axial deviatoric stress, for the axial strain rate history in Figure 1. The radial and hoop stresses are indistinguishable.

For comparison with the more conventional strain rate history considered in Figure 1, we take the rise time to the constant radial strain rate to be the same as the previous rise time to the constant axial strain rate, namely $t_1 = 135\ \mu$s; and we chose the plateau value $\dot{\lambda}_r(t_1) = 1747/s$, since this results in $\dot{e}_z(t_1) = 2500/$s. The resulting axial strain and radial stretch rates are shown in Figure 2.a. The corresponding strain and stretch acceleration histories are shown in Figure 2.b along with the normalized mean radial stress, which is nearly indistinguishable from $\ddot{\lambda}_r$. For this strain rate history, $e_z(t_1) = 0.20$ and $e_z(350\mu\text{s}) = 0.55$.

9. Numerical Simulations

To test the optimal pulse shaping and the inertial correction theory, we performed numerical simulations of hypothetical SHPB tests on a soft, nearly incompressible, solid specimen using the Lagrangean, 3-D finite element code PRESTO from Sandia Laboratories. The initial radius of the specimen was $R_0 = 6.35$ mm and the initial thickness was $L_0 = 1.45$ mm, giving a length-to-diameter ratio of 0.11. The incident and transmission bars were included in the simulation, and the specimen-bar interfaces were treated as frictionless. We used 1000 mm long aluminum bars with a radius of 19.05 mm. The specimen and bar dimensions (except for the bar lengths) were taken from the experimental study on gelatins by Moy et al. [8]. An isotropic, nonlinear elastic model was used for the specimen (a compressible version of the Mooney-Rivlin model). The model was calibrated to give rough agreement with the large strain, quasi-static, uniaxial compression data on the 20% ballistic gelatin tested in [8].[7] This resulted in a small strain shear modulus of 80 kPa. Since 20% ballistic gelatin is 80% water, we used the bulk modulus of water, 2.3 GPa; the ratio of bulk to shear modulus is 2.9×10^4.

The loading wave was generated by an imposed axial velocity history $v_z(t)$ at the far end of the incident bar. This velocity was obtained from the desired nominal axial strain rate $\dot{e}_z$ using the approximate relation

$$v_z(t) \approx \tfrac{1}{2} L_0 \dot{e}_z(t)\,, \tag{28}$$

which neglects the motion of the specimen-transmission bar interface and assumes the particle velocity doubles on reflection from the specimen-incident bar interface. The nominal axial strain rate histories used in computing $v_z(t)$ were those from Figures 1 and 2, but since the relation (28) is only approximate, the actual strain rates and strain accelerations in the specimen would differ somewhat from those in the figures even if the specimen deformation were approximately homogeneous.

Figures 3 and 4 plot the histories of $\overline{\sigma}_{zz}$, $\overline{\sigma}_{rr}$, $\overline{\sigma}_{\theta\theta}$ and $\frac{3}{2}\overline{s}_{zz}$. These are the (volumetric) mean values of the radial,

[7] Ballistic gelatin is a viscoelastic material, and the quasi-static tests showed some increase in stress with increasing strain rate. The model was calibrated so that the axial stress-strain curve was slightly above the curve for highest (quasi-static) strain rate of 1/s.

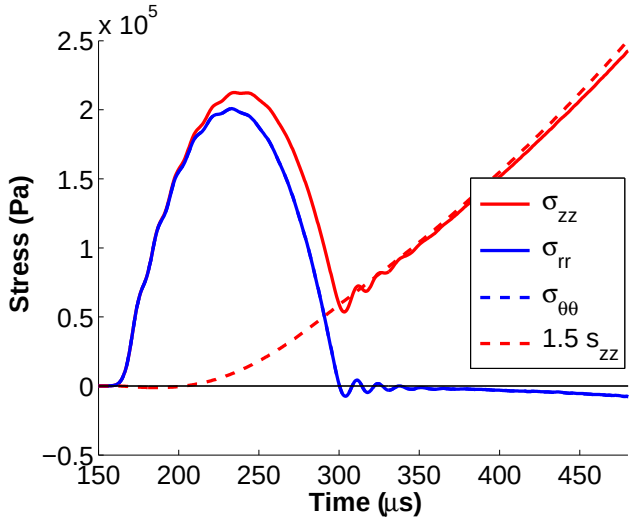

Figure 4: Mean values of the axial, radial and hoop stress and of 3/2 the axial deviatoric stress, for the axial strain rate history in Figure 2. The radial and hoop stresses are indistinguishable.

hoop and axial stress and 3/2 the mean value of the axial deviatoric stress, as computed in the simulations. Recall that $\overline{\sigma}_{zz} = \frac{3}{2}\overline{s}_{zz}$ for a uniaxial stress state; cf. $(26)_1$ with $\overline{\sigma}_{rr}$ set to zero. The times in Figures 3 and 4 are shifted relative to those in Figures 1 and 2, since in the simulations $t = 0$ is the instant at which the velocity is applied at the far end of the incident bar. Figure 3 is for a nominal axial strain rate history given (approximately) by that in Figure 1.a, that is, when $\dot{e}_z$ is eventually constant. The radial and hoop stresses are indistinguishable, and they increase substantially after the inertial spike. The compressed specimen began squeezing out beyond the bars at around 453 μs.

Figure 4 is for a nominal axial strain rate history given (approximately) by that in Figure 2.a, that is, when $\dot{\lambda}_r$ is eventually constant (an optimal pulse shape). The radial and hoop stresses are again indistinguishable, but now they drop to nearly zero after the inertial spike, that is, once $\dot{\lambda}_r$ reaches its plateau value, which occurs at a nominal strain of 0.20. Thereafter, $\overline{\sigma}_{zz}$ is very close to $\frac{3}{2}\overline{s}_{zz}$. Both of these facts indicate that a nearly uniaxial stress state has been achieved. When comparing Figures 3 and 4, keep in mind that the scales on the vertical axis are different. The inertial spike in Figure 4 is only slightly larger than that in Figure 3. For the case considered in Figures 1 and 3,

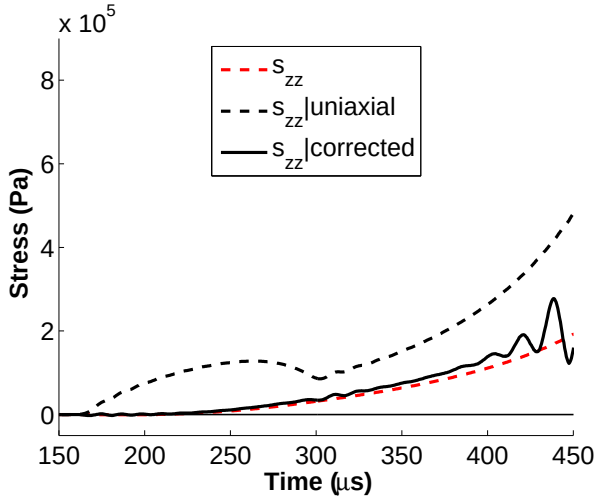

Figure 5: The computed mean axial stress (s_{zz}) compared with two estimates for it.

Figure 5 provides a check on the inertial correction $(26)_2$ for the axial deviatoric stress: $\overline{s}_{zz} = \frac{2}{3}(\overline{\sigma}_{zz} - \overline{\sigma}_{rr})$. In the

figure legend, s_{zz} denotes the mean axial deviatoric stress $\overline{s}_{zz}$ as computed in the simulation. $s_{zz}|_{\text{uniaxial}}$ denotes an estimate for the deviatoric stress that is only valid for a uniaxial stress state, namely $\frac{2}{3}\overline{\sigma}_{zz}$. It clearly disagrees with s_{zz} and shows the error that would result in neglecting inertial effects in the analysis of the data. Finally, $s_{zz}|_{\text{corrected}}$ denotes the estimate for the deviatoric stress obtained from the inertial correction above, using $\overline{\sigma}_{zz}$ computed in the simulation and $\overline{\sigma}_{rr}$ determined from $(25)_3$. It is quite close to the actual mean value for most of the simulation. Near the end of the simulation the conditions departed substantially from those on which the analysis was based: the specimen bulged and was no longer in dynamic equilibrium.

10. Discussion and Conclusions

The results of the analysis and the preliminary numerical simulations indicate that radial inertial effects in SHPB tests on soft, nearly incompressible materials could be eliminated (after a preliminary inertial spike) by tailoring the loading pulse so that the nominal *radial* strain rate in the specimen is eventually constant. The corresponding axial strain rate history is easily determined analytically and can be easily (though only approximately) imposed computationally. Whether such loading pulses can be generated experimentally with use of pulse shapers remains to be seen. Recently, Casem [14] has developed a technique for tailoring loading pulse shapes by means of graded impedance striker bars. This method, in conjunction with conventional pulse shapers, may possibly provide a means to generate the pulse shapes considered here.

References

[1] Gray III, G. T., Classic Split-Hopkinson Pressure Bar Testing. In H. Kuhn and D. Medlin, editors, *ASM Handbook Vol. 8, Mechanical Testing and Evaluation*, pages 462–476. American Society for Metals, Materials Park, Ohio, 2000.

[2] Gama, B. G., Lopatnikov, S. L. and Gillespie Jr., J. W., Hopkinson bar experimental technique: A critical review. *Appl. Mech. Rev.*, 57:223–250, 2004.

[3] Ramesh, K. T., High strain rate and impact experiments. In W. N. Sharpe, editor, *Springer handbook of Experimental Solid mechanics*, chapter 33, pages 1–30. Springer, New York, 2009.

[4] Chen, W. and Song, B., *Split Hopkinson (Kolsky) Bar*. Springer, New York, 2011.

[5] Gray III, G. T. and Blumenthal, W. R., Split-Hopkinson Pressure Bar Testing of Soft Materials. In *ASM Handbook Vol. 8, Mechanical Testing and Evaluation*, pages 488–496. American Society for Metals, Materials Park, Ohio, 2000.

[6] Chen, W., Lu, F., Frew, D. J. and Forrestal, M. J., Dynamic compression testing of soft materials. *Exp. Mech.*, 69:214–223, 2002.

[7] Song, B. and Chen, W., Split Hopkinson pressure bar techniques for characterizing soft materials. *Latin Am. J. Solids Struct.*, 2:113–152, 2005.

[8] Moy, P., Weerasooriya, T., Juliano, T. F., VanLandingham, M. R. and Chen, W., Dynamic Response of an Alternative Tissue Simulant, Physically Associating Gels (PAG). In *Proc. of the 2006 SEM Annual Conference*, 2006.

[9] Song, B., Ge, Y., Chen, W. W. and Weerasooriya T., Radial Inertia Effects in Kolsky Bar Testing of Extra-soft Materials. *Exp. Mech.*, 47:659–670, 2007.

[10] Sanborn, B., An Experimental Investigation of Radial Deformation of Soft Materials in Kolsky Bar Experiments. Master's thesis, Purdue Univ., Weast Lafayette, IN, 2010.

[11] Dharan, C. K. H. and Hauser, F. E., Determination of stress-strain characteristics at very high strain rates. *Exp. Mech.*, 10:370–376, 1970.

[12] Warren, T. L. and Forrestal, M. J., Comments on the effect of radial inertia in the Kolsky bar test for an incompressible material. *Exp. Mech.*, 50:1253–1255, 2010.

[13] Scheidler, M. and Kraft, R., Inertial effects in compression Hopkinson bar tests on soft materials. In *Proceedings of the 1st ARL Ballistic Protection Technologies Workshop*, 2010.

[14] Casem, D. T., Hopkinson bar pulse-shaping with variable impedance projectiles—an inverse approach to projectile design. Technical Report ARL-TR-5246, US Army Research Laboratory, 2010.

NO. OF COPIES	ORGANIZATION
1 (PDF only)	DEFENSE TECHNICAL INFORMATION CTR DTIC OCA 8725 JOHN J KINGMAN RD STE 0944 FORT BELVOIR VA 22060-6218
1	DIRECTOR US ARMY RESEARCH LAB IMNE ALC HRR 2800 POWDER MILL RD ADELPHI MD 20783-1197
1	DIRECTOR US ARMY RESEARCH LAB RDRL CIO LL 2800 POWDER MILL RD ADELPHI MD 20783-1197
1	DIRECTOR US ARMY RESEARCH LAB RDRL CIO MT 2800 POWDER MILL RD ADELPHI MD 20783-1197
1	DIRECTOR US ARMY RESEARCH LAB RDRL D 2800 POWDER MILL RD ADELPHI MD 20783-1197

NO. OF COPIES ORGANIZATION

10 SANDIA NATIONAL LABORATORIES
J NIEMCZURA
MS 0661
PO BOX 5800
ALBUQUERQUE NM 87185

1 ARMY RSRCH OFC
RDRL ROE M
D STEPP
RDRL ROE V
L RUSSELL
PO BOX 12211
RESEARCH TRIANGLE PARK NC
27709-2211

2 US ARMY MEDICAL RSRCH AND MATL COMMAND
BLAST INJURY RSRCH PROG COORDINATING OFC
MCMR RTB
M LEGGIERI
R GUPTA
FORT DETRICK MD 21702-5012

2 US ARMY MEDICAL RSRCH AND MATL COMMAND
DIRCTRT FOR COMBAT CASUALTY CARE
MCMR RTC
COL D HACK
D GIBSON
FORT DETRICK MD 21702-5012

1 PURDUE UNIV
AERONAUTICS AND ASTRONAUTICS
W CHEN
701 W STADIUM AVE
WEST LAFAYETTE IN 47907-2045

2 MASSACHUSETTS INSTITUTE OF TECHLGY
INSTITUTE FOR SOLDIER NANOTECHNOLOGIES
R RADOVITZKY
S SOCRATE
BLDG NE47 4TH FL
77 MASSACHUSETTS AVE
CAMBRIDGE MA 02139

1 UNIV OF FLORIDA
MECHL AND AEROSPACE ENGRNG
G SUBHASH
GAIESVILLE FL 32611

NO. OF COPIES ORGANIZATION

1 RUTGERS THE STATE UNIV OF NEW JERSEY
DIR OF FED RSRCH RELATIONS
B LAMATTINA PH D PE
96 FRELINGHUYSEN RD CORE BLDG
PISCATAWAY NJ 08854

1 NVL AIR WARFARE CTR
AIRCRAFT DIV
HUMAN SYSTEMS DEPT
B SHENDER
CODE 4656 BLDG 2187 STE 2280A
48110 SHAW RD UNIT 5
PATUXENT RIVER MD 20670-1906

2 THE JOHNS HOPKINS UNIV
DEPT OF MECHL ENGRNG
LATROBE 122
DLT K T RAMESH
DLT VY NGUYEN
3400 N CHARLES ST
BALTIMORE MD 21218

1 CFD RSRCH CORP
A J PRZEKWAS
215 WYNN DR
HUNTSVILLE AL 35805

5 THE JOHNS HOPKINS UNIV
APPLIED PHYSICS LAB
DLT T HARRIGAN
DLT A LENNON
DLT A MERKLE
DLT J ROBERTS
DLT M TREXLER
11100 JOHNS HOPKINS RD
LAUREL MD 20723-6099

1 SANDIA NATL LAB
NANOSCALE AND REACTIVE PROCESSES
S SCHUMACHER
PO BOX 5800 MS 0836
ALBUQUERQUE NM 87185-0836

1 UNIV OF NEBRASKA
N CHANDRA
114G OTHMER HALL
PO BOX 880642
LINCOLN NE 68588-0642

NO. OF COPIES ORGANIZATION

1 UNIV OF TEXAS-AUSTIN
AEROSPACE ENGRG AND
ENGRNG MECHANICS
K RAVI-CHANDAR
1 UNIV STATION C0600
AUSTIN TX 78712-0235

3 US ARMY MEDICAL RSRCH
AND MTRL CMND
JTAPIC PROG OFC
MRMC RTB
DLT F LEBEDA
DLT W LEI
DLT J USCILOWICZ
504 SCOTT ST
FORT DETRICK MD 21702-5012

1 NVL SURFACE WARFARE CTR
P DUDT
CODE 664
9500 MACARTHUR DR
WEST BETHESDA MD 20817

1 TARDEC
RDTA RS
R SCHERER
BLDG 200C RM 1150
WARREN MI 48397

1 NATICK SOLDIER RSRCH DEV
AND ENGRNG CTR
AMSRD NSC WSTB
M G CARBONI
KANSAS ST
BLDG 4 RM 247
NATICK MA 01760-5000

1 AMC NSRDEC
M CODEGA
KANSAS ST
NATICK MA 01760

1 UNIFORMED SERVICES UNIV
DEPT OF SURGERY A3020
A E DMITRIEV
4301 JONES BRIDGE RD
BETHESDA MD 20814

1 BAE SYSTEMS
R TANNOUS
9113 LE SAINT DR
FAIRFIELD OH 45014-5453

NO. OF COPIES ORGANIZATION

2 SOUTHWEST RSRCH INST
MECHL AND MTRLS ENGRNG DIV
MTRLS ENGRNG DEPT
DLT D NICOLELLA
DLT W FRANCIS
6220 CULEBRA RD
SAN ANTONIO TX 78238

1 THE UNIV OF UTAH
K L MONSON
50 S CENTRAL CAMPUS DR
2132 MERRILL ENGINEERING BLDG
SALT LAKE CITY UTAH 84112

1 MISSISSIPPI STATE UNIV
L N WILLIAMS
BOX 9632
MISSISSIPPI STATE MS 39762

1 COLUMBIA UNIV
B MORRISON
351 ENGINEERING TERRACE
MAIL CODE 8904
1210 AMSTERDAM AVE
NEW YORK NY 10027

1 APPLIED RSRCH ASSOC INC
SOUTHWEST DIV
C E NEEDHAM
4300 SAN MATEO BLVD NE
STE A 220
ALBUQUERQUE NM 87110

1 DIRECTOR
TRAUMATIC INJURY RSRCH PROG
DEPT OF MILITARY AND
EMERGENCY MEDICINE
UNIFORMED SERVICES
UNIV OF THE HEALTH SCI
P E RAPP
4301 JONES BRIDGE RD
BETHESDA MD 20814-4799

1 US ARMED FORCES
MEDICAL EXAMINER SYS
J M GETZ
1413 RSRCH BLVD
ROCKVILLE MD 20850

1 WALTER REED ARMY INST OF
RSRCH
DEPT OF BEHAVIORAL
BIOLOGY
G KAMIMORI
503 ROBERT GRANT AVE 2W97
SILVER SPRING MD 20910-7500

NO. OF COPIES ORGANIZATION

2 CTR FOR INJURY BIOMECHANICS
WAKE FOREST UNIV
MEDICAL CTR BLVD
DLT J STITZEL
DLT F S GAYZIK
WINSTON SALEM NC 27157

1 HENRY JACKSON FOUNDATION
US ARMY AEROMEDICAL RSRCH LAB
D WISE
6901 ANDREWS AVE
FORT RUCKER AL 36362-0577

ABERDEEN PROVING GROUND

1 US ARMY ABERDEEN TEST CTR
TEDT AT SLB
A FOURNIER
400 COLLERAN RD
APG MD 21005-5059

78 DIR USARL
RDRL CIH C
P CHUNG
RDRL HRS C
K MCDOWELL
K OIE
B LANCE
W HAIRSTON
J VETTEL
RDRL SL
R COATES
RDRL SLB W
W MERMAGEN
M TEGTMEYER
C KENNEDY
P GILLICH
A BREUER
L ROACH
R SPINK
A KULAGA
N EBERIUS
K RAFAELS
RDRL WML H
M FERMEN-COKER
L MAGNESS
B SCHUSTER
RDRL WMM
J ZABINSKI
RDRL WMM B
G GAZONAS
P MOY

NO. OF COPIES ORGANIZATION

RDRL WMM G
C GOLD
B LEIGHLITER
J LENHART
R MROZEK
A RAWLETT
RDRL WMP
P BAKER
S SCHOENFELD
RDRL WMP B
C ADAMS
R BECKER
S BILYK
J BRADLEY
D CASEM
J CLAYTON
A DAGRO
D DANDEKAR
A DWIVEDI
J FITZPATRICK
J GAIR
M J GRAHAM
M GREENFIELD
C A GUNNARSSON
C HOPPEL
J HOUSKAMP
Y HUANG
R KRAFT
B LEAVY
M LYNCH
D MACKENZIE
P J MCKEE
C MEREDITH
D POWELL
M RAFTENBERG
B SANBORN
S SATAPATHY
M SCHEIDLER (10 CPS)
T WEERASOORIYA
C WILLIAMS
S WOZNIAK
RDRL WMP C
T W BJERKE
RDRL WMP D
S HALSEY
RDRL WMP E
B LOVE
RDRL WMP F
E FIORAVANTE
A FRYDMAN
N GNIAZDOWSKI
R GUPTA
R KARGUS

NO. OF
COPIES ORGANIZATION

1 DSTL BIOMEDICAL SCI
A HEPPER
RM 1A BLDG 245
PORTON DOWN
SALISBURY WILTSHIRE
SP4 OJQ
UNITED KINGDOM

4 DRDC VALCARTIER
DLT K WILLIAMS
DLT A BOUAMOUL
DLT L MARTINEAU
DLT D NANDLALL
2459 PIE-XI BLVD NORTH
QUEBEC QC G3J 1X5 CANADA

1 DRDC TORONTO
C BURRELL
133 SHEPPARD AVE WEST
PO BOX 2000
TORONTO ON M3M 3B9 CANADA

1 CIMVHR
QUEENS UNIVERSITY
SCHOOL OF REHABILITATION
THERAPY
A B AIKEN
KINGSTON ON K7L3N6 CANADA

1 HUMAN PROTECTION AND
PERFORMANCE DIV
DEFENCE SCIENCE AND
TECHNOLOGY ORGANISATION
DEPARTMENT OF DEFENCE
T RADTKE
BLDG 109 506 LORIMER ST
FISHERMANS BEND VICTORIA 3207
AUSTRALIA

INTENTIONALLY LEFT BLANK.